MONTANA STATE UNIVERSITY LIBRARY

Biofilm detection in a model well-bore environment using low-field magnetic resonance

Authors: Catherine M. Kirkland, Randy Hiebert, Adrienne Phillips, Elliot Grunewald, David O. Walsh, Joseph D. Seymour, Sarah L. Codd

NOTICE: This is the peer reviewed version of the following article: Kirkland CM, Hiebert R, Phillips A, Grunewald E, Walsh DO, Seymour JD, Codd SL, "Biofilm detection in a model well-bore environment using low-field magnetic resonance," Groundwater Monitoring & Remediation 2015 Fall 35(4) 36–44, which has been published in final form at http://dx.doi.org/10.1111/gwmr.12117. This article may be used for non-commercial purposes in accordance with Wiley Terms and Conditions for Self-Archiving.

Kirkland CM, Hiebert R, Phillips A, Grunewald E, Walsh DO, Seymour JD, Codd SL, "Biofilm detection in a model well-bore environment using low-field magnetic resonance," Groundwater Monitoring & Remediation 2015 Fall 35(4) 36–44.

Made available through Montana State University's ScholarWorks
scholarworks.montana.edu

Biofilm Detection in a Model Well-Bore Environment Using Low-Field NMR

by Catherine M. Kirkland, Randy Hiebert, Adrienne Phillips, Elliot Grunewald, David O. Walsh, Joseph D. Seymour, and Sarah L. Codd

Abstract

This research addresses the challenges of the lack of non-invasive methods and poor spatiotemporal resolution associated with monitoring biogeochemical activity central to bioremediation of subsurface contaminants. Remediation efforts often include growth of biofilm to contain or degrade chemical contaminants, such as nitrates, hydrocarbons, heavy metals, and some chlorinated solvents. Previous research indicates that nuclear magnetic resonance (NMR) is sensitive to the biogeochemical processes of biofilm accumulation. The current research focuses on developing methods to use low-cost NMR technology to support in situ monitoring of biofilm growth and geochemical remediation processes in the subsurface. Biofilm was grown in a lab-scale radial flow bioreactor designed to model the near wellbore subsurface environment. The Vista Clara Javelin NMR logging device, a slim down-the-borehole probe, collected NMR measurements over the course of eight days while biofilm was cultivated in the sand-packed reactor. Measured NMR mean log T_2 relaxation times decreased from approximately 710 to 389 ms, indicating that the pore environment and bulk fluid properties were changing due to biofilm growth. Destructive sampling employing drop plate microbial population analysis and scanning electron and stereoscopic microscopy confirmed biofilm formation. Our findings demonstrate that the NMR logging tool can detect small to moderate changes in T_2 distribution associated with environmentally relevant quantities of biofilm in quartz sand.

Introduction

In most environments, the majority of microbial cells exist in complex communities called biofilms (Sutherland 2001). Bacteria preferentially attach to surfaces, anchoring themselves with a sticky gel called extracellular polymeric substance (EPS). The EPS, which consists of proteins, polysaccharides, and DNA, forms a heterogeneous matrix surrounding the bacterial cells and entrapped organic and inorganic molecules (Characklis and Marshall 1990). The EPS matrix has a complex structure, consisting of hydrated gel-like fibers and interconnected channels (Vogt et al. 2013). Depending on its physical properties, the EPS matrix can change soil pore connectivity, effective pore size, and hydraulic conductivity, thereby affecting the hydrodynamic properties of the porous media (Cunningham et al. 1991; Drescher et al. 2013; Seymour et al. 2004a).

Bioremediation methods exploit these biofilm-induced changes in the soil and can be effective to contain or degrade chemical contaminants in the subsurface (LaGrega et al. 2001). Once established, biofilm can consume hydro-carbons and other contaminants directly as a substrate (Kao et al. 2003, 2004; Komlos et al. 2004; Kim et al. 2006), induce mineralization to trap contaminants (Phillips et al. 2013), mediate ion exchange to remove heavy metals from aqueous solution (von der Schulenburg et al. 2008) or transform heavy metals to insoluble forms (Pal et al. 2008). In situ bioremediation applications often require injection of appropriate nutrients into the subsurface in order to create redox conditions suitable for biofilm growth and contami-nant transformation. In addition to being an integral part of the removal of toxins, biofilm can act as a bio-barrier to slow the migration of the contamination or re-direct groundwater flow through a treatment zone (Cunningham et al. 2003) by reducing hydraulic conductivity and restricting advective flow. Furthermore, biofilms better withstand environmental stresses such as nutrient deprivation, changing pH condi-tions, and exposure to biocides or antimicrobial substances compared to suspended cells (Mitchell et al. 2008; Petrova and Sauer et al. 2012), improving their effectiveness and longevity as bio-barriers.

Numerous computer models have been developed in the last several decades in an effort to better understand the physical and biochemical processes of biofilm devel-opment. In general, the recent models iteratively solve partially decoupled differential equations governing con-servation of momentum, mass transport, substrate utiliza-tion, and biofilm growth (Kapellos et al. 2007; Thullner and Baveye 2008; von der Schulenburg et al. 2009; Pintelon et al. 2012). The models help describe the changing hydro-dynamics and biofilm morphology, as well as confirm the overall reduced hydraulic conductivity of the porous media resulting from biofilm accumulation that is observed experimentally.

This observed reduction in hydraulic conductivity is the typical method for determining whether biofilm is present in bioremediation applications (Cunningham et al. 1990, 1991; Stewart and Fogler 2001). Darcy's Law, $v = -K\ (dh\ /\ dl)$ describes the relationship between the specific discharge, v [L/t], and the pressure gradient along a length of porous media, dh/dl [dimensionless], where the constant of proportionality is the saturated hydraulic conductivity, K [L/t]. Biofilm accumulation in pore spaces has been shown to reduce hydraulic conductivity by approximately 99% in a field setting and up to 99.99% in laboratory experiments (Stewart and Fogler 2001; Cunningham et al. 2003).

In conjunction with hydraulic conductivity measurements, determination of biofilm presence is often assessed with heterotrophic plate counts (HPC) to quantify the number of viable cells in the bulk fluid (Lazarova and Manem 1995). Interpretation of this type of population data is not trivial since the cell count data pertains to suspended bacteria rather than those attached to surfaces as biofilm. Furthermore, how the number of suspended cells correlates to the number of cells existing within biofilm colonies is not well understood. To determine cell populations within the biofilm, samples of the porous media must be collected and analyzed. Direct destructive sampling of contaminated soils during remediation can be both costly and potentially hazardous. Moreover, cell count information in general provides no information regarding the in situ physical characteristics of the biofilm, such as the thickness, structure, and density of the EPS component as this information is destroyed during sampling and plating. While these methods are useful to describe the hydraulic conductivity or biological community at a particular place and time, they are less useful for informing us about the spatial and temporal growth, maturation, and decay of the biofilm (Bayer et al. 2010).

Nuclear magnetic resonance (NMR) provides an alternative method to monitor in situ biofilm development, overcoming several of the limitations described above. The measured signal in ^{1}H NMR comes from coherently precessing hydrogen protons, or "spins," making NMR applicable for the study of materials containing water or organic matter, including biofilm (Potter et al. 1996; Hoskins et al. 1999). Previous research indicates that NMR is sensitive to the biogeochemical processes of biofilm growth (Sanderlin et al. 2013) and, unlike other methods of study, allows for non-invasive and non-destructive examination of the relationship between biofilm development and porous media hydrodynamics and mass transport over various time and length scales (Van As and Lens 2001; Seymour et al. 2004b, 2007; Gjersing et al. 2005). A fundamental understanding of these related processes is critical to optimize the effectiveness of bioremediation applications, making NMR methods a useful addition to the bioremediation monitoring toolkit.

The Vista Clara Javelin device is a slim, down-the-borehole NMR logging tool (4.5 ft (1.37 m) long, 3.5 in (8.9 cm) diameter) originally developed for hydrogeologic analysis in open or PVC-cased boreholes between 2 and 8 in (5–20 cm) in diameter (Walsh et al. 2013). Expanding from this conventional application, the research reported here uses the Javelin probe to detect changes in the signal relaxation response over time as a measurement of biofilm growth in a model sand bioreactor since biofilm accumulation enhances signal relaxation (Sanderlin et al. 2013). The method using a NMR logging tool as described in this article may provide an improved and non-destructive way to assess the subsurface presence of biofilm.

Theory

T_2 Relaxation

Following excitation with a radio-frequency (rf) pulse, the induced NMR signal decays at a rate governed by two relaxation mechanisms—spin-lattice T_1 and spin-spin T_2 (Callaghan 1991). T_1 relaxation is related to the rate at which the net magnetization grows in the longitudinal direction and returns to thermal equilibrium. T_2 relaxation is related to dipolar interactions in the transverse plane and loss of phase coherence, resulting in magnetization decay and signal attenuation.

The statistical distribution of T_2 relaxation times provides information regarding the physicochemical environments the protons experience, since environmental factors like pore fluid type and pore size control how likely protons are to experience dipolar interactions. Typically, the signal decays more rapidly in solid-like materials due to T_2 relaxation—that is, solids and gels have shorter T_2 relaxation times than liquids due to low rotational mobility enhancing dipolar coupling (Callaghan 1991). The T_2 relaxation time for pure water is on the order of 2 to 3 s in unrestricted environments, whereas it is on the order of milliseconds in porous materials due to restricted motion and surface interactions.

While both T_1 and T_2 relaxation times can provide information about the molecular and pore-scale environment, T_2 measurements require less time to conduct and are preferred. This experimental study uses measured changes in the T_2 distribution to infer changes in the pore scale environment due to biofilm growth within the bioreactor. Biofilm formation in porous media leads to shorter T_2 relaxation times (Hoskins et al. 1999; Bayer et al. 2010).

Porous media influences the NMR relaxation process in several ways. The presence of solid surfaces creates relaxation sinks and may introduce paramagnetic impurities, as well as generating susceptibility-induced magnetic field inhomogeneities. T_2 in a pore is also influenced by the viscosity and chemical properties of the bulk fluid. Furthermore, diffusion of the liquid molecules between pores, and diffusion within the pore due to local magnetic field gradients also affect the T_2 relaxation behavior of a porous media system. The expression for the rate of T_2 relaxation in porous media includes the relaxation time of the bulk media, T_{2B}, the surface relaxation time, T_{2S}, and relaxation time due to diffusion, T_{2D} (Grunewald and Knight 2011).

$$\frac{1}{T_2} = \frac{1}{T_{2,B}} + \frac{1}{T_{2,S}} + \frac{1}{T_{2,D}} \tag{1}$$

When the bulk fluid is water, $1/T_{2B}$ is typically very small and is often neglected in literature on relaxometry in porous materials. However, as the rotational mobility of the

bulk fluid decreases due to biofilm growth in the pore space, $1/T_{2B}$ increases in importance to the overall T_2 relaxation rate (Kleinberg et al. 1990). Surface relaxation, T_{2S}, depends on the surface relaxivity, ρ, which describes the efficiency of the mineral surface to enhance relaxation, and the surface to volume ratio, S/V (Brownstein 1979).

$$\frac{1}{T_{2,S}} = \rho\frac{S}{V} \tag{2}$$

Since biofilm is composed of bacterial cells in a hydrated gel matrix, the T_2 relaxation time of fluid contained in the biofilm is shorter than for the bulk fluid alone. As the biofilm grows into the pore spaces, proportionally more protons will be bound in, or interact with, the EPS matrix, thereby shifting the T_2 distribution toward shorter relaxation times. Enhanced T_2 relaxation due to biofilm formation is expected to be caused by reduced rotational mobility in the pore fluid as the EPS matrix contributes a gel phase and the cells produce biomacromolecules with shorter relaxation than bulk water (T_{2B}). Additional relaxation effects may be due to changes in the pore structure and surface due to the biofilm growth on the grain surfaces (T_{2S}) (Codd et al. 2011).

T_{2D} is directly related to the echo spacing, t_E, according to

$$\frac{1}{T_{2,D}} = D\frac{(\gamma G t_E)^2}{12} \tag{3}$$

where D is the diffusion coefficient [L^2 t^{-1}], γ is the gyromagnetic ratio of hydrogen, 2.675×10^8 rad/(T s), and G is the local effective magnetic field gradient [Gauss L^{-1}]. By selecting a short t_E, this term can be made sufficiently small as to be neglected. Repeating the experiment with a longer t_E indicates whether there are indeed enhanced relaxation effects due to diffusion to consider.

Materials and Methods

Bioreactor Design and Construction

The lab-scale bioreactor was designed to model the near-wellbore environment and was constructed inside an aluminum Faraday cage using four concentric PVC pipe sections (Titan Industries, Paxton, Nebraska), ranging from the inner 8 in (20 cm) diameter solid pipe to the outer 20 in (51 cm) solid pipe (Figure 1). The two middle pipe sections, 10 in (25 cm) and 18 in (46 cm) diameter, respectively, were screened over the entire length with 8 rows of 0.020 in (0.051 cm) wide slots spaced at 0.5 in (1.3 cm) intervals. All of the pipes were 2.5 ft (76 cm) tall. Top and bottom plates were constructed from 0.5 in (1.3 cm) high density rigid expanded PVC sheeting with machined 0.125 in (0.32 cm) concentric grooves to allow nesting and sealing of the vertical pipe sections.

The 3 in (7.6 cm) annulus between the slotted pipes was wet-filled with approximately 2.3 ft^3 (0.065 m^3.) of No. 2095 Granusil® silica (quartz) sand (Unimin Corp., Ottowa, Minnesota) having a nominal diameter of 1 mm and a porosity of approximately 0.37. The combined volume of the pore space and annular reservoirs was approximately 40 L.

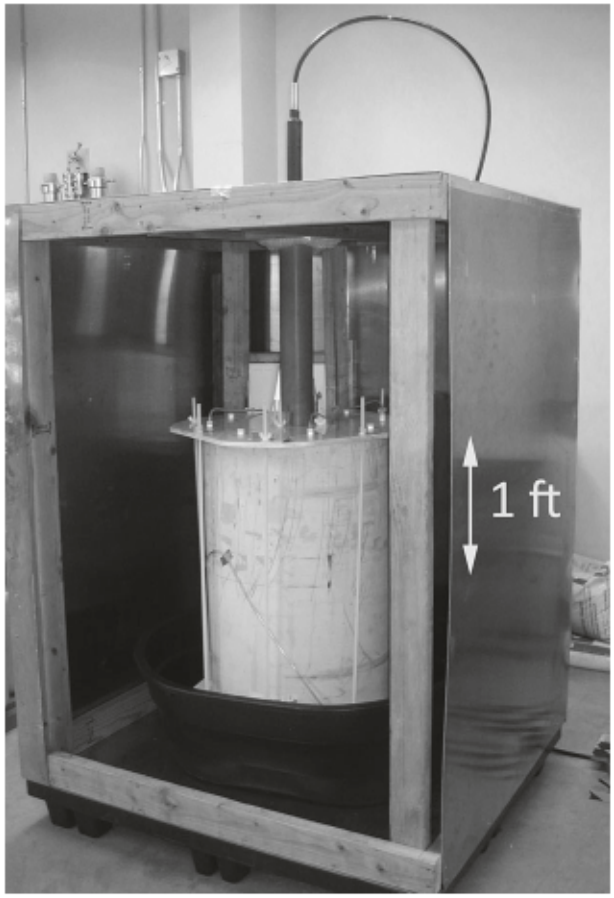

Figure 1. Model well-bore bioreactor. The 3.5 in (8.9 cm) diameter NMR logging probe was installed in the lab-scale radial flow bioreactor and Faraday cage. The purpose of the Faraday cage was to reduce external radio frequency noise caused by various electromagnetic sources in the laboratory.

The reactor was disinfected with two pore volumes (80 L) of 10% bleach solution with 7 g/L Tween80 (Fisher BioReagents, Waltham, Massachusetts) followed by a flush with 80 L sterile de-ionized (DI) water. Two pore volumes (80 L) of sterile 2.52 g/L sodium thiosulfate solution was pumped into the reactor to neutralize any remaining bleach. The sodium thiosulfate solution was flushed from the reactor with 80 L of sterile buffer solution consisting of 3 g/L $NaNO_3$, 0.12 g/L K_2HPO_4, and 0.04 g/L KH_2PO_4.

NMR measurements were made in the buffer-filled reactor with the NMR logging tool to establish a baseline T_2 distribution for the reactor prior to any biofilm growth. Later measurements were compared to this initial condition to identify changes in T_2 relaxation time distributions. Experimental constraints prevented the testing of an uninoculated control in parallel with measurements of the biofilm reactor. These constraints are primarily associated with the uncertainties that would have been introduced by moving the NMR probe between the reactors to conduct measurements. Moving the probe during the experiment could influence the results since a slightly different shell within the reactor would be excited and measured for each placement of the probe. For these reasons, a longitudinal study of a single reactor was the preferred method for this initial experiment.

Bacterial Culture

One milliliter frozen stock of *Bacillus mojavensis* was cultured in 100 mL of modified Brain-Heart Infusion (BHI) broth (36 g/L Brain Heart Infusion (BHI) (Becton, Dickinson and Co., Sparks, Maryland), 3 g/L $NaNO_3$, 0.75 g/L NH_4Cl, 40 g/L NaCl) on a shaker table at 150 rpm for 48 h. Then the 100 mL inoculum was added to 10 L of the modified BHI broth and mixed on a stir plate at 1150 rpm for 60 h to a concentration of approximately 7 $\log_{10}$ colony-forming units (cfu)/mL. *B. mojavensis* was selected because of the abundant mucoid biofilm it produces (Mitchell et al. 2008; Sanderlin et al. 2013).

The 10 L inoculum was pumped into the reactor with two peristaltic pumps (Cole-Parmer Model 7553-80 [Vernon Hills, Illinois] with Masterflex Easy-Load 7515-00 heads [Vernon Hills, Illinois]) at 650 to 700 mL/min through eight lines of No. 16 vinyl tubing. The pumps were turned off for approximately 11 h to allow the bacteria to attach to the sand. Following the attachment period, radial flow of substrate through the sand promoted bacterial growth and biofilm accumulation which was monitored by the NMR probe.

No attempt was made to maintain a *B. mojavensis* monoculture within the reactor for the duration of the experiment. Following inoculation, subsequent batches of substrate were mixed and pumped into the reactor in a non-sterile manner. Sterile conditions could not be maintained due to experimental constraints imposed by the large volumes of substrate used and waste produced daily.

Following inoculation, 40 L of re-circulating substrate was removed daily from the system and replaced with 40 L of fresh substrate. Except during no-flow NMR measurements, the substrate was re-circulated continuously at a rate of 650 to 700 mL/min which translates to a specific discharge of approximately 0.04 cm/min and a pore velocity of approximately 0.02 mm/s at the radial center of the sand annulus. This flow rate corresponds to the pore volume of the reactor being replaced every 50 to 60 min.

NMR Data Acquisition

T_2 relaxation measurements used a CPMG pulse sequence (Carr and Purcell 1954; Meiboom and Gill 1958) with excitation pulses of either 245 kHz or 290 kHz corresponding to excitation regions at 19 cm and 17 cm (7.5 in and 7 in) from the center of the probe, respectively. Each excitation shell is 0.5 m high and several millimeters thick. Eight experiments were repeated at the same time daily (Table 1). Each experiment used a repetition time, T_r, of 5 s to allow for T_1 relaxation.

Observing changes in the T_2 measurement as a function of the echo spacing t_E can provide an indication of the significance of NMR diffusion relaxation effects. Measurements were made under flow and no flow conditions to determine if the fluid flow affected the T_2 measurement. Data was also collected under two probe tuning protocols. The first held the NMR excitation frequency constant for each experiment; the second allowed the NMR instrument to auto-tune with an adjustable excitation frequency periodically within each experiment. This allowed a determination of whether changes in probe tuning affected the T_2 measurement.

Table 1

NMR Experiments with Well-Logging Probe

Exp. No.	Averages	t_E (ms)	Flow	Excitation Frequency	Duration
1	360	6.0	No	Auto-tuned	30 min
2	360	6.0	Yes	Auto-tuned	30 min
3	360	1.5	No	Constant	30 min
4	360	1.5	Yes	Constant	30 min
5	360	6.0	No	Constant	30 min
6	360	6.0	Yes	Constant	30 min
7	360	1.5	No	Auto-tuned	30 min
8	2880	1.5	Yes	Auto-tuned	4 h

The data processing software uses the inverse Laplace transform to generate a T_2 distribution for the reactor excitation shell. Because of the generally low signal to noise ratio that is typical for a low-field NMR device in natural geologic material, the Javelin data interpretation software also calculates a noise-robust parameter based on the mean amplitude of the echoes in the record CPMG. The Square of Echoes (SOE) is calculated as the squared value of the mean of echoes. A reduction in the calculated SOE over the course of the experimental period indicates that the mean value of the T_2 relaxation time is decreasing as the conductivity of the porous media in the reactor decreases.

Sampling and Imaging

A sample of re-circulating substrate was collected daily during Experiment 6 (Table 1) and immediately serially diluted and plated (Herigstad et al. 2001) to estimate the quantity of viable cells in the reactor bulk fluid. While the suspended cell counts are not directly indicative of biofilm formation, or more specifically of EPS production, they provide a general measure of growth conditions and cell population within the reactor.

On Day 8, the reactor was drained and NMR measurements were acquired using Experiment 7 parameters (Table 1). Following the measurements, the bioreactor was destructively sampled to confirm biofilm accumulation in field-relevant quantities. The sand was removed from the reactor in layers, with samples collected in sterile, preweighed 15 mL Falcon tubes for imaging and cell population analysis. The samples were collected from the NMR probe's sensitive region in the annulus center at three depths—top (6 in [15 cm] deep from the top of pipe), middle (12 to 15 in [30 to 38 cm] deep), and bottom (28 in [71 cm] deep). Six samples were collected for both population analysis with the drop plate method and imaging with stereoscopic and scanning electron microscopy.

Ten milliliter of sterile phosphate buffered saline (PBS) solution was added to each sample of sand collected for population analysis. The samples were vortexed with a Thermolyne MaxiMix II Type 37600 mixer (Dubuque, Iowa) for 30 s each, then sonicated for 2 min (Tuttnauer CSU-3, Hauppauge, New York). Prior to serial dilution and plating, each sample was again vortexed for 30 s to remove

attached bacteria from the sand particles and break up clumps of cells. Following plating, the buffer solution was poured off and the sand samples were dried at 65°C for until their masses stabilized. The mass of dry sand and the plate count from each sample indicate cfu/g sand in the reactor.

For stereoscope microscopy analysis, biofouled sand samples from the radial flow reactor and clean control sand were stained with 300 µL of 40 µM Syto 9 (Molecular Probes, Eugene, Oregon) for 30 min. The samples were rinsed with 0.2 µm filtered (VWR, Radnor, Pennsylvania) distilled water and immediately imaged at 470 nm excitation with a Niko SMZ 1500 (Nikon, Melville, New York) stereoscope equipped with an EXFO Xcite 120 fluorescence illumination system.

Additionally, images were acquired using a Zeiss Supra 55VP scanning electron microscope (Zeiss, Pleasanton, California). Sand and biofilm from the radial flow reactor and control sand samples were sputter coated with iridium and high-resolution images were taken at 1.0 kV at a working distance of 3 to 4 mm.

Results and Discussion

The experimental NMR data shows a shift in the T_2 distribution to faster decay times, indicating that the fluid properties and pore environment changed due to biofilm growth (Figure 2). No significant relaxation enhancement due to diffusion, flow, or changes in probe tuning was observed. Therefore, unless otherwise noted, the data presented was collected during Experiment 8 where the level of background noise was lowest due to the high number of averages. The mean log T_2 relaxation time decreased from approximately 710 ms following the buffer pulse to approximately 390 ms on Day 7. Figure 2 shows the signal attenuation (top) and T_2 distributions (bottom) measured during the course of testing.

Day 1 measurements were conducted in the disinfected sand pack saturated with a phosphate buffer solution using Experiment 7 parameters and 4560 averages. Measurements taken during the inoculation of the reactor with *B. mojavensis* occurred at Day 1.5. Experiments conducted on Day 2 represent the first potential measurement of attached biofilm within the reactor. The signal decay curves and T_2 distributions collected Days 3 to 5 show significant overlap. The data collected on Days 6 and 7 likewise overlap and are shown in Figure 2 as a thick solid line. The dash-dot curve in both panels shows the data obtained on Day 8 from the drained reactor (Experiment 7).

By Day 2, the CPMG signal decay curve is notably steeper and the T_2 distribution shows a narrower peak, centered at approximately 450 ms (Figure 2). These data indicate an increase in the proportion of protons experiencing faster relaxation as would be expected in the event of biofilm formation. The rate of change of the signal response decreased after Day 2, with little change recorded in the signal Days 3 to 5. The Days 6 and 7 data show a decreased signal amplitude in the top panel relative to Day 5, indicating a decrease in the measured reactor water content. The NMR measurement from the drained reactor on Day 8 reflects the presence of biofilm, as seen in the residual peak between 200 and 300 ms. The smaller peak at approximately 7 ms most likely originates from water or biofilm that is directly bound on and interacting with the sand surface. The lower amplitude of the signal from the drained reactor reflects the desaturation of the sandpack.

The measured reactor water content decreased from 37.3% at inoculation to 32.2% on Day 7. After draining the

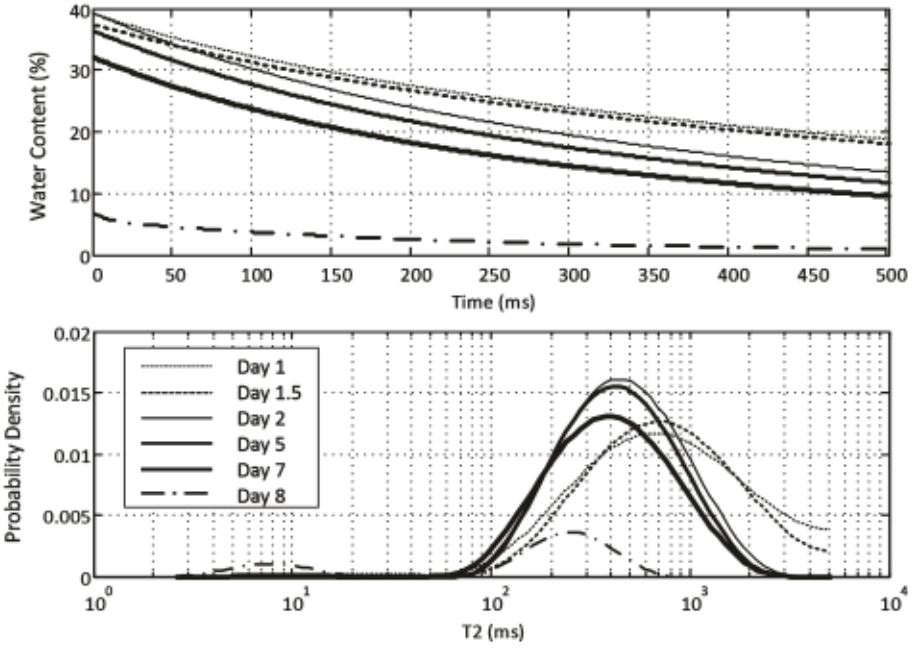

Figure 2. Time evolution of CPMG signal decay curves and T_2 distributions. Increased signal attenuation with biofilm formation produces steeper CPMG signal decay curves (top panel). The distribution of T_2 relaxation times (bottom panel) shifted to faster decay times as biofilm grew in the reactor. Data collected Days 3 and 4 overlap the Day 5 curve and are not shown. Likewise, the Day 6 data is obscured by the Day 7 curve and is not shown. Day 8 data was collected from the drained reactor.

reactor on Day 8, the measured water content was 7.0% and the mean log T_2 relaxation time was 121 ms. The decrease in measured water content during the growth phase is best explained by microbial gas production within the pores as a metabolic by-product. This biologically-driven reduction in water content of the reactor sandpack may have contributed to shorter T_2 relaxation times by increasing the effective saturated surface area to fluid volume ratio (*S/V*) in Equation 2. However, the magnitude of the T_2 shift between inoculation and Day 7 significantly exceeds that from between Day 7 and Day 8 after the reactor was drained (Figure 2). The reduction in mean log T_2 relaxation time by Day 7 was approximately 320 ms corresponding to a water content decrease of 5.1 percentage points. The 25 percentage point reduction in water content after draining the reactor produced only a further 270 ms reduction in the mean log T_2 relaxation time. T_2 relaxation times decreased nearly six times more on a water content basis [ms/% water] during the growth phase as compared to when the reactor was drained. This suggests that decrease in water content in the reactor during the experiment was likely *not* the primary mechanism causing the observed shift in the T_2 relaxation distribution. The best explanation for the observed decrease in T_2 relaxation times is biofilm accumulation in the reactor sandpack.

The measured SOE, normalized with respect to water content squared, decreased 53% between Day 1 and Day 7 (Figure 3). The normalized SOE value shows the same trends as observed in the signal attenuation and T_2 distribution data in Figure 2, where the initial change is most significant followed by stabilization in the signal response.

HPC of the daily samples show an initial drop in cfu numbers after inoculation, followed by a steady increase over the duration of the experiment (Figure 4). From an inoculum concentration on the order of 7 $\log_{10}$ cfu/mL injected into the reactor on Day 1.5, the Day 2 HPC yielded colony counts of approximately 5.5 $\log_{10}$ cfu/mL. Combined with the NMR results showing a decrease in T_2 relaxation times over the same period, this decline in HPC can be attributed to bacterial attachment and initial biofilm

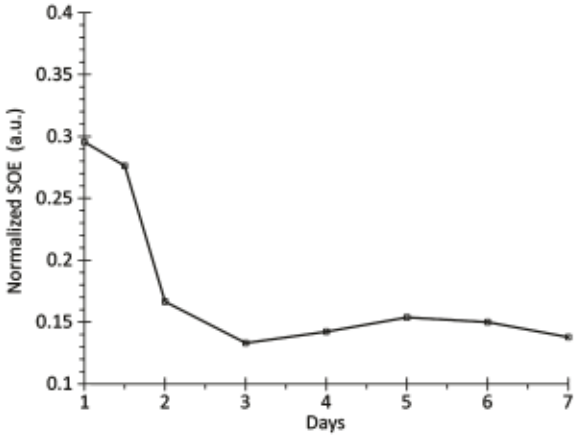

Figure 3. SOE reduction. Data for the set of long-average experiments shows a decrease of approximately 53% in the squared value of the mean of echoes over the duration of the experiment.

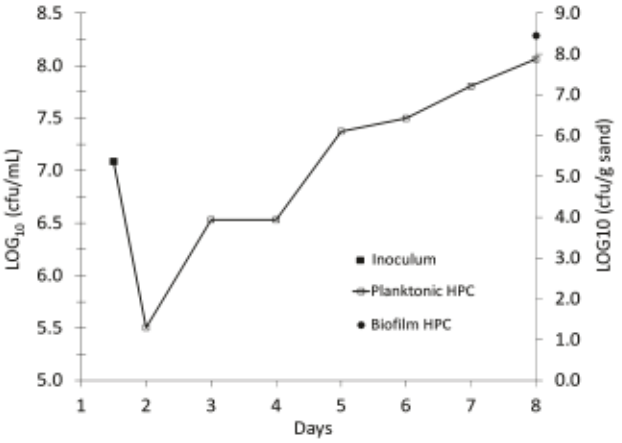

Figure 4. Heterotrophic plate counts (HPC). Daily HPC data shows a strong initial attachment of cells from approximately 7 $\log_{10}$ cfu/mL in the 10 L inoculum to 5.5 $\log_{10}$ cfu/mL on Day 2. Increasing colony numbers resulted in a final population of approximately 8 $\log_{10}$ cfu/mL by Day 8. The average biofilm HPC from the sand samples was approximately 8.5 $\log_{10}$ cfu/g sand, shown on the secondary axis.

formation on the sand particles. Planktonic cells increased in number to approximately 6.5 $\log_{10}$ cfu/mL on Days 3 and 4. These higher colony counts correspond to enhanced signal attenuation and decreases in the mean log T_2 relaxation time, though they are necessarily *not* a measurement of the cell numbers in the biofilm. The increase in SOE observed around Day 5 may correspond to a biofilm sloughing event since HPC from Day 5 were nearly an order of magnitude higher than those from Day 4, 7.4 $\log_{10}$ vs. 6.5 $\log_{10}$ cfu/mL, respectively. After Day 5, a slower rate of increase in colony numbers was observed than between Days 4 and 5, suggesting a secondary attachment period may have occurred. This interpretation is supported by the NMR data which shows a decrease in the normalized SOE over the same period. In general, the HPC data and the diverse colony morphologies indicate that conditions in the bioreactor were favorable for mixed population bacterial growth.

When the bioreactor was drained and destructively sampled, the sand was sticky, consistent with presence of a biofilm bridging the pore spaces of the sand. Cell population analysis of sand samples indicates that attached bacterial concentrations in the bioreactor were approximately 7 $\log_{10}$ to 9 $\log_{10}$ cfu/g dry sand, with an average in the reactor of 8.5 $\log_{10}$ cfu/g sand. This concentration is similar to cell counts noted in the literature for subsurface biofilms used to degrade trace organics, where populations are typically in the range of 6 $\log_{10}$ to 9 $\log_{10}$ cfu/g soil (Potter et al. 1996; Cunningham et al. 2003).

SEM images (Figure 5) showed a mixed bacterial population of rod and cocci cells, with thicker EPS at the bottom of the reactor where the fresh nutrient supply entered the reactor. Compared to samples collected in the middle and upper regions of the reactor (Figure 5a), individual cells were less distinguishable on samples collected from the bottom due to the thicker EPS matrix (not shown). Stereoscopic microscopy qualitatively confirmed the presence of biofilm on and between sand particles (Figure 5b), where the matrix

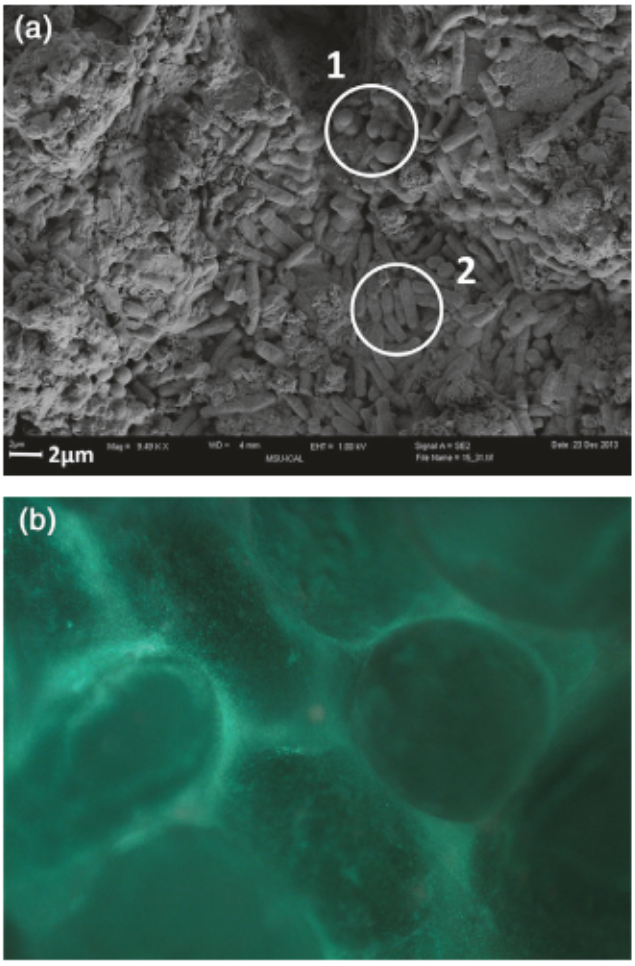

Figure 5. Porous media microscopy confirmed biofilm accumulation in the region of the reactor where NMR data was collected. (a) Scanning electron microscope (SEM) image of mixed population bacterial cells and extracellular polymeric substance (EPS) on a sand particle collected from the middle depth of the reactor. Region 1 shows cocci bacteria while Region 2 shows rod-like cells. *Bacillus mojavensis* is a rod-shaped bacteria. Depth 15 in. Scale bar is 2 µm. (b) Stereoscope image of EPS encasing the bacterial cells and binding grains of 1 mm sand. Depth 15 in. 40× magnification.

fluoresces in green and the cells are visible as bright flecks. Microscopy confirms bacterial growth and EPS production within the reactor.

Population analysis indicates both quantity and diversity of heterotrophic bacteria present without directly accounting for the presence of EPS. Microscopy of the sand can confirm the presence of the EPS matrix, but does little to elucidate the in situ characteristics and hydrodynamics of the biofouled pore space. For these reasons, characterizations of observed biofilm accumulation are qualitative and indicative of EPS formation within the NMR logging tool's sensitive region but are not intended to quantify the total amount of EPS formed in the reactor.

Several studies have demonstrated that biofilm growth in soils and rock reduces the hydraulic conductivity and permeability of the media, often by several orders of magnitude (Taylor et al. 1990, 1991; Cunningham et al. 1991, 2003). Furthermore, biofilm itself is a porous media with an internal architecture that includes voids and channels (Stoodley et al. 1994, 2002; Allison 2003). The enhanced NMR relaxation observed in this study could be due to the changing surface properties if the biofilm coats the porous media, represented as an increase in $1/T_{2S}$. However, if the biopolymers are distributed throughout the pore volume then the faster relaxation could be dominated by exchange of protons between the water and the biopolymers, which would be represented as an increase in $1/T_{2B}$.

NMR studies on T_2 decay in porous media typically focus on the influence of T_{2S} and T_{2D} on the overall relaxation behavior of the medium (Kleinberg et al. 1993, 1994; Godefroy 2001; Anand and Hirasaki 2008). When the bulk fluid in the pore space changes, however, as it does during biofilm formation, the influence of T_{2B} can no longer be neglected. In the bulk phase, the production of polymer-like EPS and biomacromolecules will enhance spin relaxation as protons bound to the polymers and dissolved organics rapidly exchange with free protons on the liquid molecules (Hills et al. 1991). This relaxation mechanism produces shorter relaxation times than would be expected in bulk water. As the content of EPS and biomacromolecules increases within the pore space relative to the initial condition, the weighted average of "bound" and "free" proton T_2 times will shift in the direction of the polymer relaxation time to shorter T_2 decay times (Codd et al. 2011; Vogt et al. 2013).

From a macroscopic perspective, biofilm may act as a relatively impermeable surface, insofar as it is restrictive to convective flow within pores. At the molecular level, however, biofilm is composed of approximately 97% water (Hornemann et al. 2008). For these reasons, we attribute the change in relaxation behavior observed in this experiment primarily to changes in the bulk relaxation of the pore fluid, which includes both a liquid and polymer-gel phase. In these experiments it is proposed that an increase in $1/T_{2B}$ is the best way to conceptualize the observed enhancement in the NMR T_2 relaxation.

These experiments demonstrate that a commercially available low-cost NMR logging tool can detect small to moderate changes in T_2 distribution due to biofilm accumulation in quartz sand under laboratory conditions. Mean log T_2 relaxation times decreased from 710 ms when the reactor contained a sterile buffer solution to 389 ms following 7 days of biofilm cultivation. Over the same period, the noise-robust SOE parameter decreased by 53%, indicating an increase in signal attenuation and shorter T_2 relaxation times. Normalizing the data with respect to water content squared in the reactor indicates that the change in T_2 is not primarily driven by the saturation state of the porous media in the reactor, but rather by biofilm accumulation. HPC suggest that planktonic cells in the reactor increased in abundance from approximately 5.5 $\log_{10}$ cfu/mL on Day 2 to 8 $\log_{10}$ cfu/mL on Day 8. Population data from destructive sampling confirmed colony counts of attached cells on the order of 8 $\log_{10}$ cfu/g dry sand. Scanning electron and stereoscope microscopy confirmed the presence of the biofilm matrix attached to the sand particles compared to control sand. Our results, therefore, show that the measured shift in the reactor T_2 relaxation distribution toward faster signal decay times is best explained by biofilm accumulation in the reactor pore spaces.

Our findings have the potential to improve monitoring methods for bioremediation applications involving the use of bio-barriers to slow the flow of groundwater or consume chemical contaminants. Deploying an array of the NMR probes in wells in the bio-barrier zone and recording signal changes over time could provide another measure of the robustness of the bio-barrier with respect to depth. Preparations are underway to use the NMR logging tool in situ to detect biofilm formation at an engineered field site in Butte, Montana. Considerations for this future work include the effects of moving the probe between measurements and potential influences of soil mineralogy and water chemical parameters that would likely be encountered in a natural setting.

Acknowledgments

This material is based upon work supported by the U.S. Department of Energy, Office of Science under Award Number DE-FG02-11ER90025. Any opinions, findings, and conclusions or recommendations expressed in this material are those of the author(s) and do not necessarily reflect the views of the Department of Energy. This material is based upon work supported by the National Science Foundation Graduate Research Fellowship Program under Grant DGE-1049562. The authors thank Andrew Bender, Laura Boegli, Garth James, and Ann Willis at the Center for Biofilm Engineering for assistance with the biofilm growth protocol development.

References

Allison, D.G. 2003. The biofilm matrix. *Biofouling* 19, no. 2: 139–150.

Anand, V., and G.J. Hirasaki. 2008. Paramagnetic relaxation in sandstones: Distinguishing T1 and T2 dependence on surface relaxation, internal gradients and dependence on echo spacing. *Journal of Magnetic Resonance* 190: 68–85.

Bayer, J.V., F. Jaeger, and G.E. Schaumann. 2010. Proton nuclear magnetic resonance (NMR) relaxometry in soil science applications. *Open Magnetic Resonance Journal* 3: 15–26.

Brownstein, K.R., and C.E. Tarr. 1979. Importance of classical diffusion in NMR studies of water in biological cells. *Physical Review A* 19, no. 6: 2446–2453.

Callaghan, P.T. 1991. *Principles of Nuclear Magnetic Resonance Microscopy*. New York: Oxford University Press.

Carr, H.Y., and E.M. Purcell. 1954. Effects of diffusion on free precession in nuclear magnetic resonance experiments. *Physical Review* 94, no. 3: 630–638.

Characklis, W.G., and K.C. Marshall, ed. 1990. *Biofilms*. New York: John Wiley & Sons, Inc.

Codd, S.L., S.J. Vogt, J.A. Hornemann, A.J. Phillips, J.E. Maneval, K.R. Romanenko, L. Hansen, A.B. Cunningham, and J.D. Seymour. 2011. NMR relaxation measurements of biofouling in model and geological porous media [in English]. *Organic Geochemistry* 42, no. 8: 965–971.

Cunningham, A.B., R.R. Sharp, R. Hiebert, and G. James. 2003. Subsurface biofilm barriers for the containment and remediation of contaminated groundwater. *Bioremediation Journal* 7, no. 3–4: 151–164.

Cunningham, A.B., W.G. Characklis, F. Abedeen, and D. Crawford. 1991. Influence of biofilm accumulation on porous-media hydrodynamics. *Environmental Science & Technology* 25, no. 7: 1305–1311.

Cunningham, A.B., E.J. Bouwer, and W.G. Characklis. 1990. Biofilms in porous media (Chap. 18). In *Biofilms*, ed. W.G. Characklis and K.C. Marshall, 697–732. New York: John Wiley & Sons, Inc.

Drescher, K., Y. Shen, B.L. Bassler, and H.A. Stone. 2013. Biofilm streamers cause catastrophic disruption of flow with consequences for environmental and medical systems. *Proceedings of the National Academy of Sciences of the United States of America* 110, no. 11: 4345–4350.

Gjersing, E.L., S.L. Codd, J.D. Seymour, and P.S. Stewart. 2005. Magnetic resonance microscopy analysis of advective transport in a biofilm reactor. *Biotechnology and Bioengineering* 89, no. 7: 822–834.

Godefroy, S., Korb, J.-P., Fleury, M., Bryant, and R.G. 2001. Surface nuclear magnetic relaxation and dynamics of water and oil in macroporous media. *Physical Review E* 64: 021605-1–021605-13.

Grunewald, E., and R. Knight. 2011. A laboratory study of NMR relaxation times in unconsolidated heterogeneous sediments. *Geophysics* 76, no. 4: G73–G83.

Herigstad, B., M. Hamilton, and J. Heersink. 2001. How to optimize the drop plate method for enumerating bacteria. *Journal of Microbiological Methods* 44, no. 2: 121–129.

Hills, B.P., C. Cano, and P.S. Belton. 1991. Proton NMR relaxation studies of aqueous polysaccharide systems. *Macromolecules* 24, no. 10: 2944–2950.

Hornemann, J.A., A.A. Lysova, S.L. Codd, J.D. Seymour, S.C. Busse, P.S. Stewart, and J.R. Brown. 2008. Biopolymer and water dynamics in microbial biofilm extracellular polymeric substance. *Biomacromolecules* 9, no. 9: 2322–2328.

Hoskins, B.C., L. Fevang, P.D. Majors, M.M. Sharma, and G. Georgiou. 1999. Selective imaging of biofilms in porous media by NMR relaxation. *Journal of Magnetic Resonance* 139, no. 1: 67–73.

Kao, C.M., K.F. Chen, Y.L. Chen, T.Y. Chen, and W.Y. Huang. 2004. Biobarrier system for remediation of tce-contaminated aquifers. *Bulletin of Environmental Contamination and Toxicology* 72, no. 1: 87–93.

Kao, C.M., Y.L. Chen, S.C. Chen, T.Y. Yeh, and W.S. Wu. 2003. Enhanced pce dechlorination by biobarrier systems under different redox conditions. *Water Research* 37, no. 20: 4885–4894.

Kapellos, G.E., T.S. Alexiou, and A.C. Payatakes. 2007. Hierarchical simulator of biofilm growth and dynamics in granular porous materials. *Advances in Water Resources* 30, no. 6–7: 1648–1667.

Kim, G., S. Lee, and Y. Kim. 2006. Subsurface biobarrier formation by microorganism injection for contaminant plume control. *Journal of Bioscience and Bioengineering* 101, no. 2: 142–148.

Kleinberg, R.L., W.E. Kenyon, and P.P. Mitra. 1994. Mechanism of NMR relaxation of fluids in rock. *Journal of Magnetic Resonance Series A* 108: 206–214.

Kleinberg, R.L., S.A. Farooqui, and M.A. Horsfield. 1993. T(1)/T(2) ratio and frequency-dependence of NMR relaxation in porous sedimentary rocks [in English]. *Journal of Colloid and Interface Science* 158, no. 1: 195–198.

Kleinberg, R.L., and M.A. Horsfield. 1990. Transverse relaxation processes in porous sedimentary rock. *Journal of Magnetic Resonance* 88, no. 1: 9–19.

Komlos, J., A.B. Cunningham, A.K. Camper, and R.R. Sharp. 2004. Biofilm barriers to contain and degrade dissolved trichloroethylene. *Environmental Progress* 23, no. 1: 69–77.

LaGrega, M.D., P. L. Buckingham, and J.C. 2001. Evans. *Hazardous Waste Management*. 2nd ed. New York: McGraw-Hill.

Lazarova, V., and J. Manem. 1995. Biofilm characterization and activity analysis in water and waste-water treatment. *Water Research* 29, no. 10: 2227–2245.

Meiboom, S., and D. Gill. 1958. Modified spin-echo method for measuring nuclear relaxation times. *Review of Scientific Instruments* 29, no. 8: 688–691.

Mitchell, A.C., A.J. Phillips, M.A. Hamilton, R. Gerlach, W.K. Hollis, J.P. Kaszuba, and A.B. Cunningham. 2008. Resilience of planktonic and biofilm cultures to supercritical CO2 [in English]. *Journal of Supercritical Fluids* 47, no. 2: 318–325.

Pal, A., and A.K. Paul. 2008. Microbial extracellular polymeric substances: Central elements in heavy metal bioremediation. *Indian Journal of Microbiology* 48, no. 1: 49–64.

Petrova, O.E., and K. Sauer. 2012. Sticky situations: Key components that control bacterial surface attachment. *Journal of Bacteriology* 194, no. 10: 2413–2425.

Phillips, A.J., R. Gerlach, E. Lauchnor, A.C. Mitchell, A.B. Cunningham, and L. Spangler. 2013. Engineered applications of ureolytic biomineralization: A review. *Biofouling* 29, no. 6: 715–733.

Pintelon, T., R.R., C. Picioreanu, M.C.M. van Loosdrecht, and M.L. Johns. 2012. The effect of biofilm permeability on bioclogging of porous media. *Biotechnology and Bioengineering* 109, no. 4: 1031–1042.

Potter, K., R.L. Kleinberg, F.J. Brockman, and E.W. McFarland. 1996. Assay for bacteria in porous media by diffusion-weighted NMR. *Journal of Magnetic Resonance. Series B* 113: 9–15.

Sanderlin, A.B., S.J. Vogt, E. Grunewald, B.A. Bergin, and S.L. Codd. 2013. Biofilm detection in natural unconsolidated porous media using a low-field magnetic resonance system. *Environmental Science & Technology* 47, no. 2: 987–992.

Seymour, J.D., J.P. Gage, S.L. Codd, and R. Gerlach. 2007. Magnetic resonance microscopy of biofouling induced scale dependent transport in porous media. *Advances in Water Resources* 30, no. 6–7: 1408–1420.

Seymour, J.D., J.P. Gage, S.L. Codd, and R. Gerlach. 2004a. Anomalous fluid transport in porous media induced by biofilm growth. *Physical Review Letters* 93, no. 19.

Seymour, J.D., S.L. Codd, E.L. Gjersing, and P.S. Stewart. 2004b. Magnetic resonance microscopy of biofilm structure and impact on transport in a capillary bioreactor. *Journal of Magnetic Resonance* 167: 322–327.

Stewart, T.L., and H.S. Fogler. 2001. Biomass plug development and propagation in porous media. *Biotechnology and Bioengineering* 72, no. 3: 353–363.

Stoodley, P., K. Sauer, D.G. Davies, and J.W. Costerton. 2002. Biofilms as complex differentiated communities. *Annual Review of Microbiology* 56: 187–209.

Stoodley, P., D. Debeer, and Z. Lewandowski. 1994. Liquid flow in biofilm systems. *Applied and Environmental Microbiology* 60, no. 8: 2711–2716.

Sutherland, I.W. 2001. Biofilm exopolysaccharides: A strong and sticky framework. *Microbiology* 147: 3–9.

Taylor, S.W., and P.R. Jaffe. 1991. Enhanced in-situ biodegradation and aquifer permeability reduction. *Journal of Environmental Engineering-ASCE* 117, no. 1: 25–46.

Taylor, S.W., and P.R. Jaffe. 1990. Biofilm growth and the related changes in the physical properties of a porous medium. 1. Experimental investigation. *Water Resources Research* 26, no. 9: 2153–2159.

Thullner, M., and P. Baveye. 2008. Computational pore network modeling of the influence of biofilm permeability on bioclogging in porous media. *Biotechnology and Bioengineering* 99, no. 6: 1337–1351.

Van As, H., and P. Lens. 2001. Use of H-1 NMR to study transport processes in porous biosystems. *Journal of Industrial Microbiology & Biotechnology* 26, no. 1–2: 43–52.

Vogt, S.J., A.B. Sanderlin, J.D. Seymour, and S.L. Codd. 2013. Permeability of a growing biofilm in a porous media fluid flow analyzed by magnetic resonance displacement-relaxation correlations. *Biotechnology and Bioengineering* 110, no. 5: 1366–1375.

von der Schulenburg, D.A.G., T.R.R. Pintelon, C. Picioreanu, M.C.M. Van Loosdrecht, and M.L. 2009. Johns. Three-dimensional simulations of biofilm growth in porous media. *AIChE Journal* 55, no. 2: 494–504.

von der Schulenburg, D.A.G., D.J. Holland, M. Paterson-Beedle, L.E. Macaskie, L.F. Gladden, and M.L. Johns. 2008. Spatially resolved quantification of metal ion concentration in a biofilm-mediated ion exchanger. *Biotechnology and Bioengineering* 99, no. 4: 821–829.

Walsh, D., P. Turner, E. Grunewald, H. Zhang, J.J. Butler, E. Reboulet, S. Knobbe, T. Christy, J.W. Lane, C.D. Johnson, T. Munday, and A. Fitzpatrick. 2013. A small-diameter NMR logging tool for groundwater investigations. *Ground Water* 51, no. 6: 914–926.

Biographical Sketches

C.M. Kirkland *is from Center for Biofilm Engineering, Montana State University, Bozeman, MT and Department of Chemical and Biological Engineering, Montana State University, Bozeman, MT.*

R. Hiebert *is from Center for Biofilm Engineering, Montana State University, Bozeman, MT.*

A. Phillips *is from Center for Biofilm Engineering, Montana State University, Bozeman, MT.*

E. Grunewald *is from Vista Clara Inc., 12201 Cyrus Way Ste. 104, Mukilteo, WA.*

D.O. Walsh *is from Vista Clara Inc., 12201 Cyrus Way Ste. 104, Mukilteo, WA.*

J.D. Seymour *is from Center for Biofilm Engineering, Montana State University, Bozeman, MT and Department of Chemical and Biological Engineering, Montana State University, Bozeman, MT.*

S.L. Codd, *corresponding author, is from Center for Biofilm Engineering, Montana State University, Bozeman, MT and Department of Mechanical and Industrial Engineering, Montana State University, Bozeman, MT; (406) 994 1944; fax (406) 994 6292*